JGR Atmospheres

RESEARCH ARTICLE
10.1029/2023JD039141

Elucidating the Impacts of Various Atmospheric Ventilation Conditions on Local and Transboundary Ozone Pollution Patterns: A Case Study of Beijing, China

Lian Zong[1], Yuanjian Yang[1], Haiyun Xia[1], Jinlong Yuan[1], and Min Guo[1,2]

[1]Collaborative Innovation Centre on Forecast and Evaluation of Meteorological Disasters, Key Laboratory for Aerosol-Cloud-Precipitation of China Meteorological Administration, School of Atmospheric Physics, Nanjing University of Information Science & Technology, Nanjing, China, [2]Ningxia Meteorological Information Centre, Ningxia, China

Key Points:

- Local sources are a major contributor to O_3 pollution in the whole of Beijing
- The transboundary O_3 pollution patterns are closely regulated by the wind field within the boundary layer
- Nocturnal low-level jet (LLJ) results in horizontal transport and a temporary rise in O_3 concentration, while daytime LLJ may cause a lag in peak O_3 in downwind areas

Supporting Information:

Supporting Information may be found in the online version of this article.

Correspondence to:

Y. Yang and H. Xia,
yyj1985@nuist.edu.cn;
hsia@ustc.edu.cn

Citation:

Zong, L., Yang, Y., Xia, H., Yuan, J., & Guo, M. (2023). Elucidating the impacts of various atmospheric ventilation conditions on local and transboundary ozone pollution patterns: A case study of Beijing, China. *Journal of Geophysical Research: Atmospheres*, *128*, e2023JD039141. https://doi.org/10.1029/2023JD039141

Received 24 APR 2023
Accepted 9 SEP 2023

Author Contributions:

Conceptualization: Yuanjian Yang
Data curation: Lian Zong, Jinlong Yuan
Formal analysis: Lian Zong, Yuanjian Yang, Jinlong Yuan, Min Guo
Funding acquisition: Yuanjian Yang
Investigation: Lian Zong, Yuanjian Yang
Methodology: Lian Zong, Yuanjian Yang, Jinlong Yuan, Min Guo
Project Administration: Yuanjian Yang
Resources: Yuanjian Yang
Software: Lian Zong, Jinlong Yuan, Min Guo
Supervision: Yuanjian Yang, Haiyun Xia
Validation: Lian Zong, Haiyun Xia, Jinlong Yuan, Min Guo
Visualization: Lian Zong
Writing – original draft: Lian Zong

Abstract The ventilation condition in the atmospheric boundary layer, which varies with the synoptic pattern, is a crucial factor affecting the transport and dispersion of air pollutants. In this study, taking Beijing as an example, local ozone (O_3) accumulation and the transboundary O_3 pollution (TOP) patterns during the warm season were explored under different boundary layer ventilation conditions by using integrated objective weather classification, non-negative matrix factorization, and backward trajectory model. Results show that local sources are a major contributor to O_3 pollution in the whole of Beijing, accounting for ~73.36% of the O_3 concentration on average. The local accumulation is mainly facilitated by poor ventilation conditions with weak wind speeds (<3 m/s) under favorable photochemical reaction conditions and abundant precursors, resulting in local O_3 events. In contrast, the occurrence of synoptic patterns associated with TOP is more frequent, so the TOP contribution cannot be ignored, especially for the northern regions, where it may exceed 50%. Horizontal wind vector variations play a marked role in driving the TOP, affecting not only the location of the source region and transport pathway but also the transport distance and volume. In addition, a strong nocturnal low-level jet (LLJ) results in horizontal transport and a temporary rise in O_3 concentration, while a daytime LLJ stimulates a peak in O_3 concentration over the downwind area, lagging by about 1 hr. Our findings provide new perspectives on the effects of boundary layer ventilation on the regulation of O_3 pollution, as well as other air pollutants.

Plain Language Summary The ventilation condition in the boundary layer plays an essential role in the transport and dispersion of air pollutants, and it is also an important indicator for urban air-quality forecasts. To identify the impacts of various ventilation conditions on local and transboundary ozone pollution (TOP) patterns, this study integrated objective weather classification, non-negative matrix factorization, and backward trajectory model to clarify the characteristics of TOP and quantify the contributions of local ozone (O_3) accumulation and TOP under different weather pattern in Beijing. Generally, local sources are the primary source of O_3 pollution throughout Beijing, accounting for an average of 73.36% of O_3 concentrations. Local O_3 accumulation events are triggered by poor ventilation conditions with weak wind speeds under favorable photochemical reaction conditions and abundant precursors. In comparison, the occurrence of weather patterns associated with TOP are more frequent, so the TOP contribution cannot be ignored, where it may exceed 50% for the northern regions. The TOP patterns are closely regulated horizontally and vertically by the wind vector within the boundary layer. Additionally, nocturnal low-level jet (LLJ) results in horizontal transport and a temporary rise in O_3 concentration, while daytime LLJ may cause a lag in peak O_3 in downwind areas.

1. Introduction

Tropospheric ozone (O_3) is a secondary pollutant generated by a complex series of photochemical reactions of precursors such as nitrogen oxides (NOx), carbon monoxide (CO), and volatile organic compounds under intense sunlight radiation (Gvozdić et al., 2011; Sillman, 1999). Tropospheric O_3 not only affects atmospheric oxidation and participates in the chemical transformation processes of various air pollutants, but also poses risks to human health, ecosystems, and urban construction (Pancholi et al., 2018; Yue et al., 2017). Short-term exposure to high O_3 may cause coughing and breathing difficulties, and prolonged exposure may even result in death related to respiratory and cardiovascular disease (Atkinson et al., 2012; Heal et al., 2013). In the latest global air quality guidelines issued by the World Health Organization, a level of 60 μg/m^3 [the average of maximum daily average

Writing – review & editing: Lian Zong, Yuanjian Yang, Haiyun Xia, Jinlong Yuan, Min Guo

8-hr O_3 concentrations (MDA8 O_3)] is recommended for peak season O_3 based on all non-accidental mortality and respiratory mortality (WHO, 2021). As a dominant component of atmospheric oxidants, O_3 reacts with gaseous and particulate pollutants emitted into the boundary layer to generate secondary aerosols which, because of their strong oxidative properties, lead to photochemical pollution. The state of air pollution in China has markedly improved since 2013 as a result of the implementation of the Air Pollution Prevention and Control Action Plan by central and local governments; however, the problem of O_3 pollution in summer is gradually raising awareness amongst the public (Lu et al., 2018; Song et al., 2017; Zong et al., 2022).

Unlike other atmospheric pollutants, tropospheric O_3 is not a primary pollutant emitted directly into the atmosphere; its production is mainly determined by precursors and photochemical reaction conditions (strong solar radiation and high temperatures) (Kley et al., 1994; Sillman, 1999). Consequently, O_3 accumulation always occurs during the daytime, and serious O_3 pollution is more likely to be observed during the warm season (Lam et al., 2005; Lu et al., 2018). Additionally, numerous observations have revealed that higher O_3 concentrations are not only apparent in individual cities, but also at regional scales (Fu et al., 2019; Z. Zhao & Wang, 2017). In addition to the contribution of local precursor emissions and meteorological conditions, the transportation of O_3 and its precursors plays an essential part in O_3 pollution (Deng et al., 2019; M. Y. Wang et al., 2020). For instance, Wang et al. (2022) illustrated that O_3 and its precursors accumulated in the Yangtze River Delta (YRD) can be transported to the Pearl River Delta (PRD) urban agglomeration under the influence of the outflow of typhoons, which results in regional transport contributing 53.5% of the O_3 formation over the PRD.

In general, with certain precursor emissions, the formation of O_3 depends to a large extent on whether the weather situation provides favorable conditions for photochemical reactions and pollutant dispersion (T. Wang et al., 2017). Many studies have previously investigated the synoptic circulation situations that contribute to high O_3 levels, revealing for instance that the strength of the East Asian summer monsoon and western Pacific typhoon activities correlate positively with the surface O_3 in southern China (Deng et al., 2019; C. Zhao et al., 2010). Other studies have explored the meteorological variables of O_3 pollution based on multiple linear regression modeling (W. Chen et al., 2022; Gvozdić et al., 2011), among which W. Chen et al. (2022) proposed a new index called the meteorology synthetic index to quantify ground-level O_3 pollution induced by the meteorological conditions with consideration given to both the photochemical reaction conditions and the physical dispersion capacity. Additionally, some previous studies have suggested that synoptic forcing can induce transboundary air pollutant transport from adjacent regions to downwind areas, such as southerly winds blowing aerosols from southern industrial cities (e.g., Shijiazhuang, Cangzhou, and Baoding) to Beijing (C. Liu et al., 2022; Miao et al., 2017). Similarly, southwesterly transportation pathways are associated with most PM_{10} pollution in Beijing (F. Wang et al., 2010), and the response of O_3 pollution to approaching typhoons is characterized by strong regional transportation (Shao et al., 2022; N. Wang et al., 2022). Zong et al. (2022) identified a weather pattern that favors the transport of O_3 and precursors to Beijing, but the detailed transport characteristics have not yet been clarified (i.e., the transport source regions, pathways, and relative contributions).

In the last two decades, several novel methodologies for classifying synoptic circulation fields have been applied to comprehensively investigate the atmospheric circulation mechanisms underlying the various O_3 distribution patterns. These methods include *k*-means clustering, principal component analysis (PCA), empirical orthogonal function analysis, and self-organizing maps (Han et al., 2020; Huth et al., 2008; Yin et al., 2019). Consequently, it has been possible to classify meteorological fields according to the subject and object of the study and categorize similar situations into homogeneous groups, thereby facilitating the improved study of their meteorological mechanisms. Hence, it is also a possibility that the horizontal wind fields of O_3 pollution events can be classified to fully interpret the regulation of O_3 concentrations by horizontal transport characteristics.

Chemical transport models are commonly used in efforts to understand the mechanisms and quantify the contributions of the transport of pollutants. However, they are computationally expensive and carry several uncertainties rooted in the emission inventories employed and their representation of chemical mechanisms (Foley et al., 2015; Lu et al., 2019). Meanwhile, several mathematical (statistical) methods have also been demonstrated as capable of classifying source types and quantity contributions, with the help of some robust source identification methods (Kim & Park, 2007; M. Luo et al., 2018). For example, the scheme proposed by Luo et al. (2018), which incorporates non-negative matrix factorization (NMF) with pollution-rose and backward trajectory models to estimate the contribution of transboundary pollution, can provide robust results on the temporal and spatial variations of transboundary air pollutants.

In this study, we integrated objective weather classification, NMF analysis, and backward trajectories to assess local-scale O_3 accumulation and the characteristics of transboundary O_3 pollution (TOP) arising from regional-scale horizontal wind fields in the boundary layer (Section 3.1), together with local 3D wind field observations from Doppler wind Lidar to interpret the boundary layer wind field characteristics of typical cases of O_3 pollution (Section 3.2). Section 4 provides some corresponding discussion of the results, followed by a summary of our main conclusions in Section 5.

2. Data and Methods

2.1. Air Quality Data and Meteorological Data

Hourly ground-level O_3 observational data were retrieved from the China Environmental Monitoring Station, ultimately comprising 714 stations in North China and 35 stations in Beijing after data quality control. To investigate the effect of atmospheric circulation on precursor transport, here we similarly used hourly CO and NO_2 data from the above stations. In addition, these 35 stations in Beijing are categorized into urban, traffic, suburban, and rural stations based on their subsurface properties and location in the city, including 9 for urban stations, 14 for suburban stations, 5 for traffic stations (road monitoring stations for traffic air quality), and 7 for rural stations (for more details, see Figure S1 and Text S1 in Supporting Information S1). The hourly data from meteorological stations in China were obtained from the China Meteorological Data Service Centre, including observational values of such weather elements as temperature, pressure, relative humidity, wind, total cloud cover, and precipitation. In addition, some gridded meteorological data, such as downward ultraviolet radiation at the surface (UV), boundary layer height (BLH), and geopotential height and horizontal wind at 925 hPa, from ERA5 hourly reanalysis data with a horizontal resolution of 0.25° latitude × 0.25° longitude, were collected from the European Centre for Medium-Range Weather Forecasts.

2.2. Doppler Wind Lidar Observation

To analyze the modulation of TOP by local wind fields, we further explored the 3D wind fields and O_3 distribution in Beijing based on single coherent Doppler wind Lidar (CDWL) observations at Beijing Daxing International Airport from 2021-05-12 to 2021-07-12. As already mentioned, the dominant TOP in Beijing is from the cities to the south (F. Wang et al., 2010; Zong et al., 2022), so Beijing Daxing International Airport (location: 39.48°N, 116.4°E), located in the southernmost part of Beijing (Figure S1 in Supporting Information S1), is an appropriate site for capturing the wind field characteristics for southerly TOP. The CDWL works with a spatial and temporal resolution of 30 m and 0.2 s, respectively, in each beam at an eye-safe wavelength of 1.5 μm [for more details on the CDWL, refer to Yuan et al. (2022)]. Continuous wind profiles and the turbulent kinetic energy dissipation rate (TKEDR), every 10 min, within the troposphere up to an altitude of 6 km, were derived from the CDWL based on velocity azimuth display scans, and the mixed layer height could be identified at a TKEDR threshold of 10^{-4} m^2 s^{-3} (Banakh et al., 2020; Wang et al., 2021). Additionally, since turbulence is locally isotropic within the inertial range, and its structure obeys the 2/3 Kolmogorov–Obukhov law, the structure-function of the radial velocity within the inertial subrange depends only on the TKEDR (Kolmogorov, 1991). In this case, the TKEDR can be estimated by the turbulence statistical model with the relation between the structure-function of the radial velocity measured by the lidar and theoretical radial velocity structure-function (Banakh & Smalikho, 2018; Smalikho & Banakh, 2017; Yang et al., 2019).

2.3. T-Mode Principal Component Analysis

T-mode principal component analysis (T-PCA), an objective method for classifying time series of weather patterns by obliquely rotated principal components, can categorize similar weather patterns into homogeneous groups. In this study, we determined the number of classifications by a higher explained cluster variance difference between adjacent numbers of classifications that substantially improved performance and stability. For more details on the T-PCA algorithm, please refer to Huth (2000) and Miao et al. (2017). T-PCA can accurately reflect the characteristics of the original circulation pattern, without drastic variations owing to any adjustment of the classification object. Therefore, the spatiotemporal characteristics of the results are also more stable. T-PCA has been widely used in analyzing the synoptic patterns of various extreme weather and pollution, such as the weather circulation patterns that are prone to the formation of $PM_{2.5}$ pollution in winter (Ning et al., 2019; Yang et al., 2018) and O_3 pollution in summer (Dong et al., 2020; Zong et al., 2022), the meteorological mechanisms

of the combined high $PM_{2.5}$ and O_3 pollution (Y. Luo et al., 2022; Zong et al., 2021), winter monsoon patterns for urban heat island intensity (Yang et al., 2022), and the large-scale western Pacific subtropical high circulation for summer precipitation events in eastern China (Yang et al., 2021), etc. In this study, the horizontal wind fields (u and v components; range: 32°–47°N, 110°–125°E, 0.25° × 0.25°) at 925 hPa on O_3 pollution days during 2015–2021 in Beijing were selected as the samples for classification.

2.4. NMF

NMF is a matrix factorization that decomposes all elements into non-negative values and achieves a nonlinear dimensionality reduction, resulting in a more interpretable and reasonable outcome (Brunet et al., 2004; Lee & Seung, 1999). Furthermore, NMF can identify the contributions of different emission sources to air pollutants without a series of chemical composition data. As NMF is a fully mathematical (statistical) decomposition, it should also be used in conjunction with methods that can provide a scientific and robust interpretation (M. Luo et al., 2018). Here, given a non-negative O_3 concentration matrix A ($n \times m$, where n is the number of observations and m is the number of stations), NMF decomposes A into two non-negative output matrixes, as follows:

$$A_{n\times m} = W_{n\times r} \times H_{r\times m}. \tag{1}$$

Matrix W ($n \times r$, where r is the number of NMF factors) is the composition of each factor, and matrix H ($r \times m$) is the contribution of each factor (Malley et al., 2014). The iterative solution of NMF starts with random initial values and ends with the minimum Euclidean distance between A and $W{\cdot}H$. In this study, we set r to 2, decomposing O_3 concentrations into local and TOP sources. In addition, we ran the NMF algorithm 200 times to enhance the stability of the factorization.

2.5. Concentration Weighted Trajectory Analysis

Concentration weighted trajectory (CWT) analysis can assign a weighted concentration to each grid cell by averaging the sample concentrations and coupling them to the trajectories that passed through the grid cells, as follows (Y. Q. Wang et al., 2009):

$$C_{ij} = \frac{1}{\sum_{l=1}^{m} \tau_{ijl}} \sum_{l=1}^{m} C_l \tau_{ijl}, \tag{2}$$

where C_{ij} is the average weighted concentration in the grid cell (i, j), l is the index of the trajectory, m is the total number of trajectories, C_l is the air pollutant concentration measured at the endpoint on trajectory l, and τ_{ijl} is the time spent in the grid cell (i, j) for trajectory l. The weighted concentration field displays the concentration gradient for the potential concentration with high C_{ij} values, indicating that airflow over the grid (i, j) is related to high concentrations at the receptor. Additionally, the trajectories in the CWT analysis were obtained from a 72-hr backward particle dispersion simulation by the HYSPLIT model based on meteorological data from the Global Data Assimilation System.

2.6. Random Forest Model

The Random Forest (RF) model is one of the most popular and efficient machine learning algorithms available. RF is an analytical method for assessing the importance of variables with a decision tree approach, which provides a better fit to nonlinear data than traditional methods (H. Wang et al., 2019; Xiao et al., 2018). The specific details of the RF model construction process can be referred to in S. Chen et al. (2022) and Zeng et al. (2020). To overcome the problem of unilateral test results and insufficient training data, a 10-fold cross-validation method was used to validate the RF model by dividing the sample into 10 subsets, with 9 subsets used for model training and one retained to test the accuracy of the model. Ensuring that each subset was used once for testing, the average of 10 repeated cross-validation results was considered as the final prediction result. Then, the predictive performance of the RF model was assessed by the coefficient of determination and root-mean-square error. Finally, the "Mean Decrease Accuracy" and "Mean Decrease Gini" were used to evaluate the importance of each variable, with higher values indicating greater importance (H. Wang et al., 2019).

Based on the RF model, the temperature and relative humidity at 2 m, wind speed at 10 m, BLH, UV, precipitation, total cloud cover, and ventilation coefficient (*Ven*) were used as input boundary layer meteorological variables to determine their importance to total O_3 and its local and TOP sources. Specifically, *Ven* is a parameter

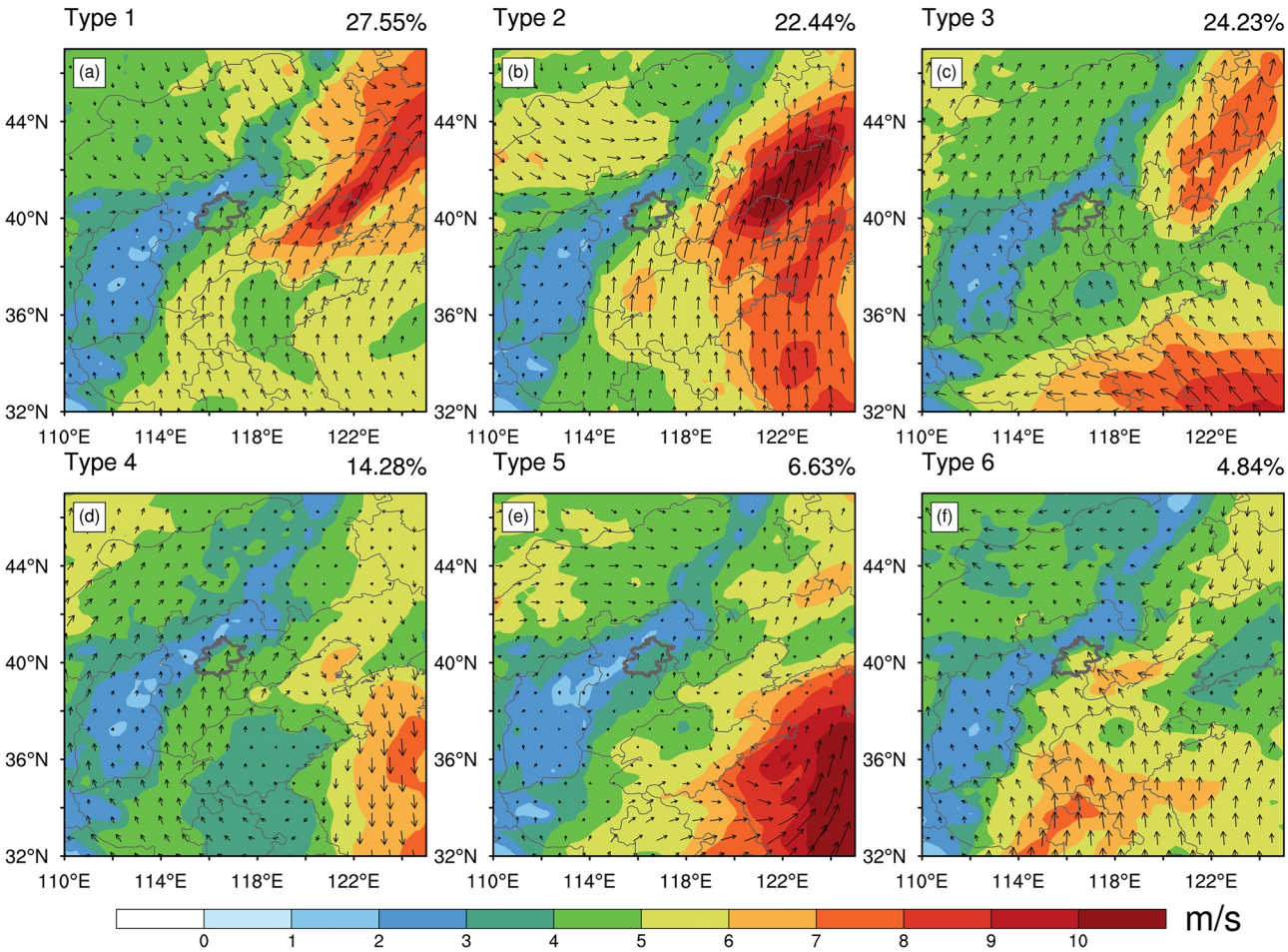

Figure 1. Regional-scale wind circulation pattern characteristics of regulating O_3 pollution events in Beijing during 2015–2021 at 925 hPa from ERA5 reanalysis data (gray outline represents Beijing, and the number in the upper-right corner of each panel indicates the frequency of occurrence of each pattern).

indicating the ventilation of the boundary layer, of which a large value favors the diffusion of pollutants (Qi et al., 2015). *Ven* can be described as follows:

$$Ven = \frac{1}{1000}\int_0^{BLH} \sqrt{u_i^2 + v_i^2}\, dZ_i, \tag{3}$$

where u_i and v_i are the zonal and meridional wind components at the ith layer, respectively.

3. Results

3.1. Modulation of O_3 Pollution by Regional-Scale Wind Vectors

3.1.1. O_3 Pollution Events Related to Various Regional-Scale Wind Fields

To begin with, we investigated all O_3 pollution days in Beijing during 2015–2021, and there were a total of 392 days with an average MDA8 O_3 above 160 μg/m^3. Six dominant wind field patterns at 925 hPa from ERA5 reanalysis data were identified by using T-PCA as follows: (a) Type 1, southernly winds (~6 m/s) and north-westerly winds (<5 m/s) converge to the northeast of Beijing (42°N, 118°E); (b) Type 2, southernly winds (~7 m/s) and north-westerly winds (~6 m/s) converge to the north of Beijing (41°N, 116°E); (c) Type 3, south-easterly winds (~5 m/s) prevail in the Beijing–Tianjin–Hebei (BTH) region; (d) Type 4, southerly winds (~5 m/s) prevail in the BTH region; (e) Type 5, light southerly winds (~3 m/s) prevail in Beijing and surrounding cities; (f) Type 6, southernly winds (~7 m/s) and northeasterly winds (~6 m/s) converge in Beijing (Figure 1).

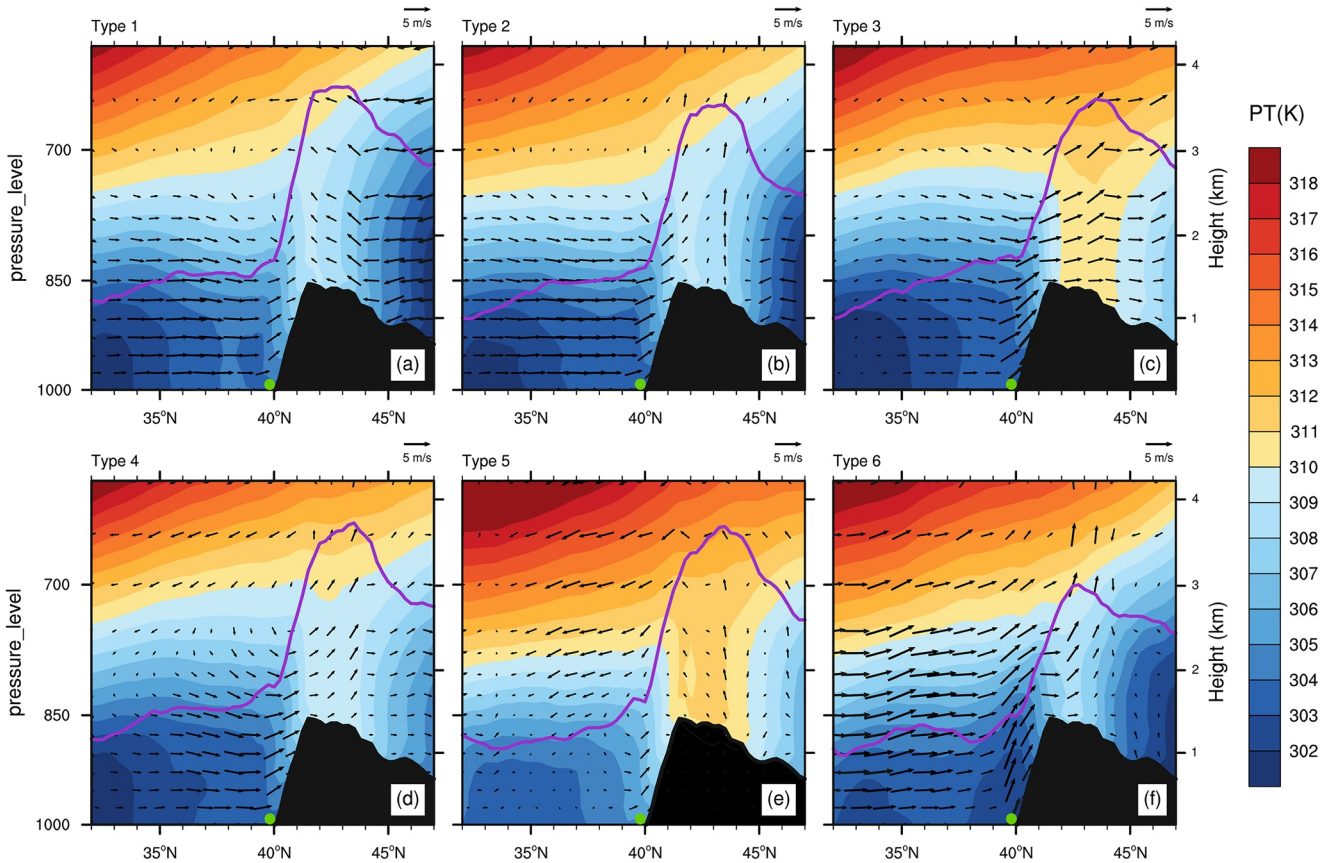

Figure 2. Vertical cross-sections of the potential temperature (contours) and wind vectors (synthesized by v and ω scaled by 100) averaged between 116.0°E and 117.0°E associated with the wind patterns at 14:00 BJT from ERA5 reanalysis data (purple solid lines mark the BLH, black contours mark the topography, and the green dot marks the location of Beijing).

Furthermore, we also focused on the 850-hPa synoptic circulation field corresponding to six patterns (Figure S2 in Supporting Information S1). At 850 hPa, both Type 1 and Type 2 show that the north is controlled by low pressure and the south is controlled by high pressure, but the convergence of Type 1 is more to the northeast. For Type 3, there is a weak high pressure located east of Beijing to induce a south-eastward transport, but for Type 4 the high pressure is located south of Beijing, resulting in the accumulation of pollutants in Beijing and the southern areas. Under Type 5, the wind speed in Beijing is relatively weak owing to the impact of the uniform pressure field, which suppresses the transport from other regions and local sources are dominant. And for Type 6, Beijing is located between two high-pressure systems, with north-eastward and south-eastward air currents jointly transported to Beijing.

Figure 2 shows the south–north vertical cross-section of wind vectors at 14:00 Beijing time (BJT) for six patterns. The wind within the boundary layer in the area south of Beijing is characterized by strong southerly wind with weak vertical mixing under Type 1; whereas the ascending motion from Beijing to the north gradually intensifies, and the pollutants are trapped in Beijing as the BLH decreases under Type 2. Type 3 and Type 6 are associated with light vertical mixing and a lower BLH in northern Beijing, suppressing the continued transport of pollutants out to the north; but for Type 4, the elevated BLH and updrafts may be accompanied by some pollutant exportation. Under Type 5, the horizontal and vertical wind speeds are quite low, and the stability of the boundary layer in Beijing and southern areas is not conducive to the dispersion of pollutants.

3.1.2. TOP Characteristics Induced by Regional-Scale Wind Fields

In addition to the regional ventilation conditions, the concentrations of pollutants in the upwind area are another important factor in determining the TOP. Figure 3, Figures S3 and S4 in Supporting Information S1 show the distributions of MDA8 O_3, NO_2, and CO concentrations in the BTH region under different wind patterns, respectively. Together with

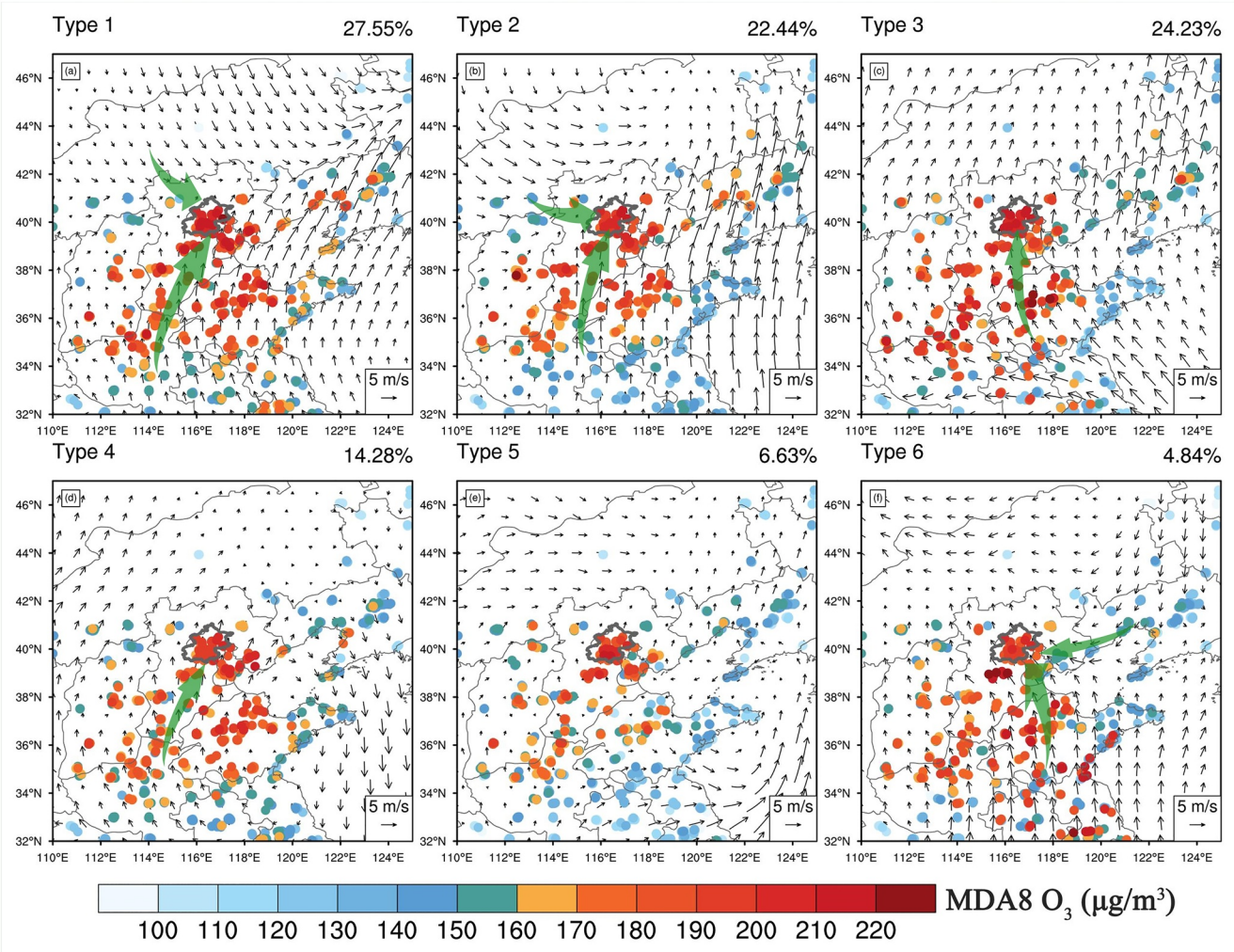

Figure 3. Characteristics of the wind field (black arrows) and MDA8 O_3 (scatter points) distribution under six patterns (green arrows indicate transport pathways, and their thickness indicates the magnitude that can be transported).

the horizontal wind field properties, the TOP characteristics under the six patterns are specified in Table 1. Notably, long-distance transport and precursor transport are also significant contributors to excessive O_3 pollution in Beijing. Specifically, although TOP contributions from the west under Type 2 and from the north under Type 6 in Beijing are relatively insignificant, the larger NO_2 and CO can be transported from the upwind region to Beijing by boundary layer winds, and Type 6 is accompanied by super-regional transportation from the YRD. Furthermore, the potential source contribution areas based on CWT analysis were identified, as shown in Figure 4. Local transport, intraregional transport, and interregional transport are discussed here concerning Shu et al. (2019), showing remarkable TOP differences under different weather patterns. Here the Lidar station is considered as the center, and divides the regional boundaries into local, intra-regional, and inter-regional with the boundaries of the regions in the ranges of 0–110 km, 110–220 km, and 220–550 km, respectively. In detail, Type 1 is characterized by 37.10% local transport, 32.66% intra-regional transport from south-central Hebei Province, and 22.81% inter-regional transport from central Shanxi Province and southern Hebei Province. For Type 2, local, intra-regional, and inter-regional (northern Shanxi Province and northern Henan Province) transport contribute 31.54%, 35.42%, and 33.04%, respectively. The TOP of Type 3 is dominated by parallel local, intra-regional, and inter-regional transport (northern Henan Province and northern Shandong Province). Local and intra-regional transport is dominant for the TOP of Type 4. For the stable Type

Table 1
The TOP Characteristics Under Six Patterns

Wind pattern	TOP characteristics
Type 1	Southwestern O_3 + CO + NO_2; Northwestern O_3
Type 2	Southern O_3 + CO, Western CO + NO_2
Type 3	Southeastern O_3 + CO + NO_2
Type 4	Southwestern O_3 + CO + NO_2
Type 5	Less local transport
Type 6	Southeastern O_3 + CO; Northeastern CO + NO_2

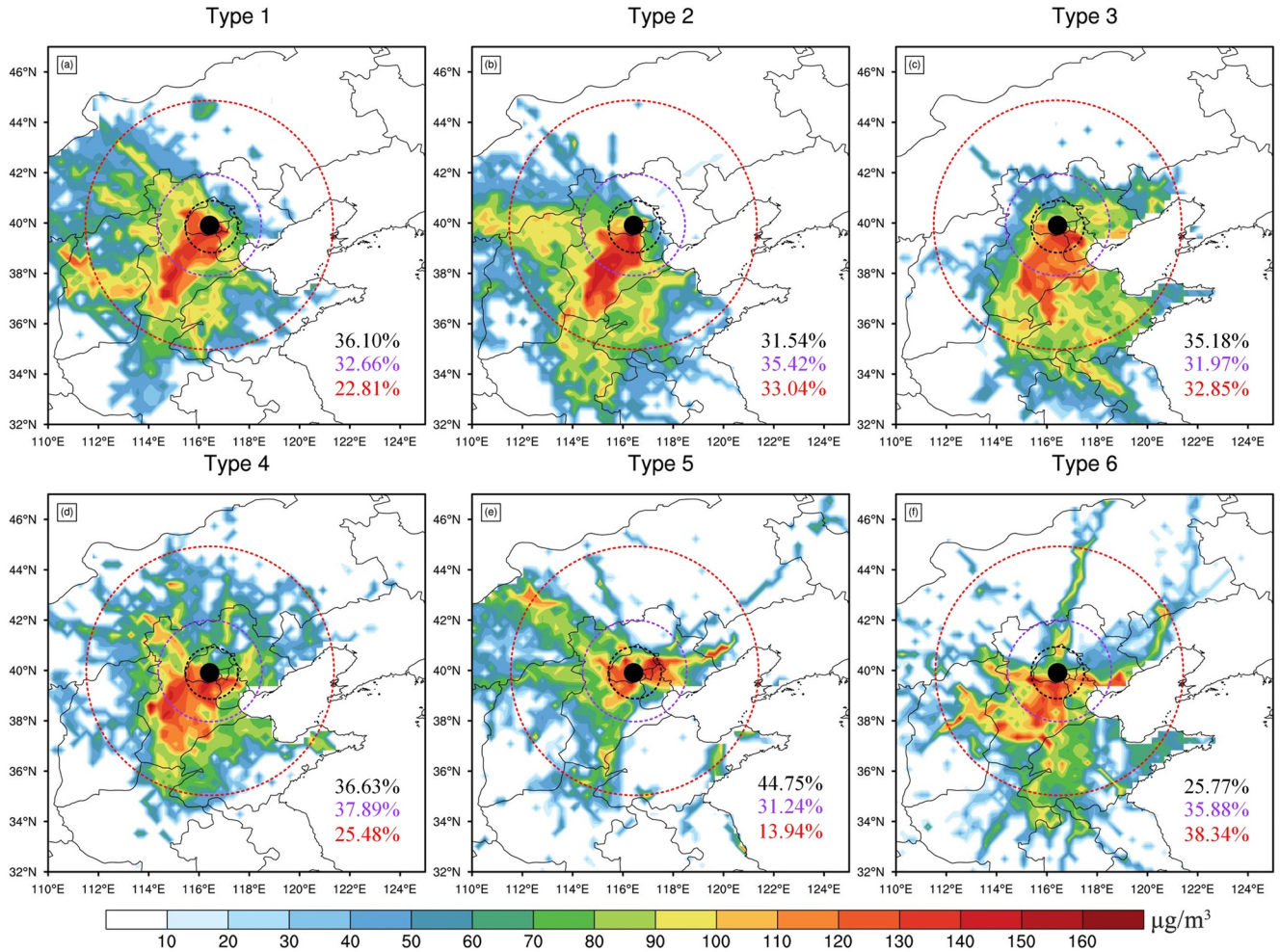

Figure 4. Potential source contribution distribution of O_3 pollution in Beijing under six patterns based on CWT analysis. The black solid line, purple dotted line, and red dashed line indicate local transport, intra-regional transport, and inter-regional transport, respectively, and the numbers of corresponding colors indicate their contribution rates.

5, there is 44.75% local transport and 31.24% intra-regional transport, while 38.34% inter-regional transport (central Shanxi Province and northern Shandong Province) and 35.88% intra-regional transport comprises the majority of TOP under Type 6. The maximum transport height extending from the surface to about 650 hPa in the north-western TOP is dominated by Type 1; whereas, in comparison, pollutants transported to Beijing in other directions occur throughout the entire atmospheric layer lower than 850 hPa. In particular, the southeastern TOP during Type 3 and Type 6 remains from the surface up to 950 hPa, which is significantly lower than for the other patterns (Figure S5 in Supporting Information S1). Table 2 illustrates the contributions of local and TOP sources under the six patterns based on 200 NMF decompositions, considering that local sources (~74.25%) are the major cause of O_3 pollution in Beijing under certain precursor emissions, which is similar to the results of a previous study (M. Y. Wang et al., 2019).

Moreover, Figure S6 in Supporting Information S1 reveals that the most important meteorological factors regulating O_3 pollution are first temperature and radiation, which influence photochemical reaction conditions for O_3 production, followed by atmospheric stability, ventilation, and other factors. As a result, the boundary layer wind field induced by the synoptic circulation pattern not only influences the local photochemical reaction conditions but also contributes substantially to the TOP feature differences. Type 1, 3, and 4 are favorable to intra-regional TOP; Type 2 and 6 mainly have higher inter-regional transport; and Type 5 mainly consists of local sources (Figure 4). It is also notable that the overall source contribution is relatively similar under the six patterns (Table 2), and differences in TOP contribution

Table 2
The Contribution of TOP and Local Sources Under Six Patterns Based on 200 NMF Decompositions

Sources	Type 1	Type 2	Type 3	Type 4	Type 5	Type 6
TOP	27.12%	24.63%	28.30%	27.73%	23.80%	25.04%
Local	72.88%	75.37%	71.70%	72.27%	76.20%	74.96%

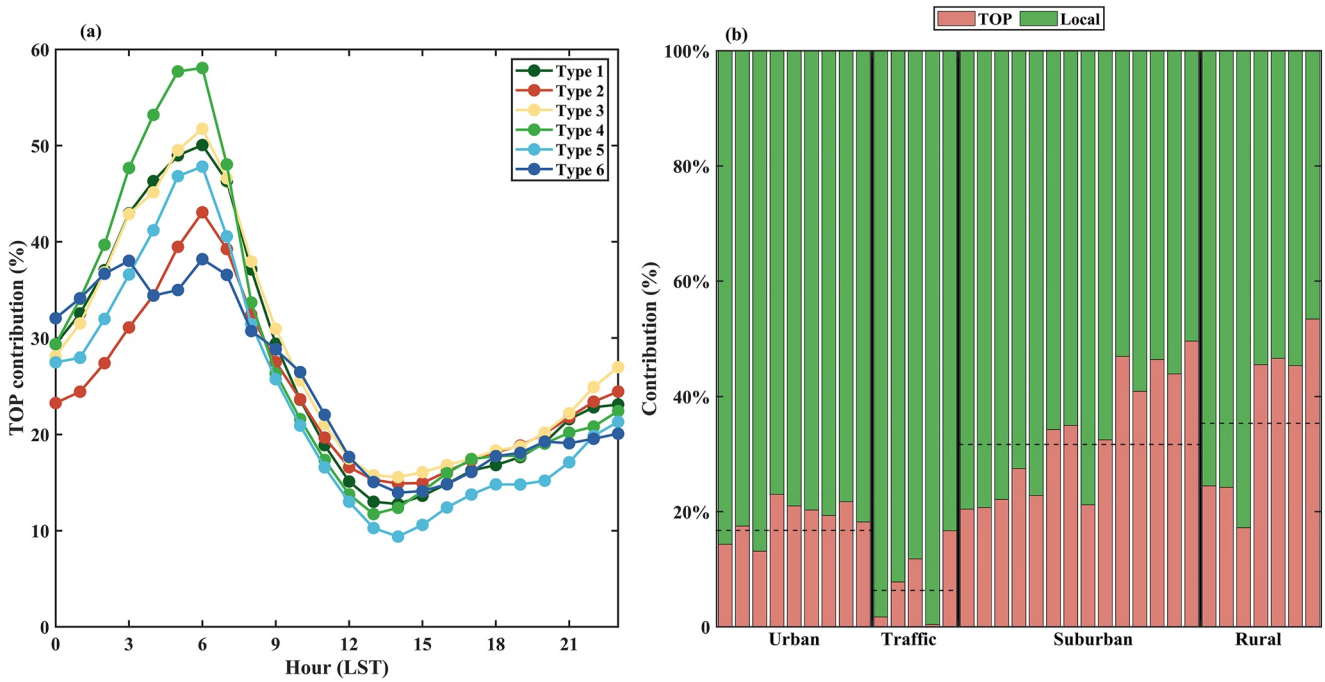

Figure 5. (a) The diurnal variation of TOP contributions in Beijing under six patterns based on NMF results. (b) Percentages of NMF factor contributions for each type of station in Beijing (each type of station is ranked from left to right according to its latitudinal position from south to north).

induced by synoptic patterns mainly occur in the early morning, with TOP peaking after sunrise (Figure 5a); the contributions of different stations are more dependent on the subsurface and latitudinal position of the station (Figure 5b). More specifically, traffic stations are least affected by TOP (~8%) owing to higher precursor emissions, whereas suburban and rural areas are much more sensitive to TOP. In addition, as the location changes from south to north, the contribution from TOP tends to rise gradually; the pollutants would be trapped in the northern areas under the obstruction of the Yanshan Mountains (to the north of Beijing). Note that while there are minor variations in the overall TOP source contribution rates for the six patterns, their transport pathways and TOP source region characteristics are clearly distinguishable.

Figure 6 indicates the top five most important meteorological factors under each pattern modulating the total O_3, local source, and TOP source according to the RF model (see Figures S7 and S8 in Supporting Information S1 for the predictive performance). The most critical meteorological factors regulating O_3 pollution are temperature, relative humidity, and solar UV radiation associated with the photochemical reaction environment. In terms of TOP, the importance of BLH, which symbolizes the atmosphere's environmental capacity, and *Ven*, which represents the ventilation condition in the boundary layer, increases significantly concerning the overall O_3. Better ventilation is more conducive to the transport of pollutants and precursors to Beijing under Type 3, which has the highest TOP source contribution (Table 2). In contrast, under Type 5, where the local source concentration is considered greater, a lower BLH and light wind speed lead to poor ventilation conditions that are not favorable for pollutant dispersion. Local variations in boundary layer meteorological elements account for the major differences in spatial patterns of O_3 under different wind patterns.

3.2. Modulation of O_3 Pollution by Local Winds

Based on wind profile Lidar observations at Beijing Daxing International Airport, it was found that the dominant wind directions at 500 m corresponding to O_3 pollution days in Beijing are mainly southerly and northeasterly (Figure S9 in Supporting Information S1 and Figure 7a). Furthermore, the MDA8 O_3 in Beijing and the upwind region under the dominant wind direction during the observation period are depicted in Figure 7. In particular, the WS at 500 m during O_3-polluted days was 4–8 m/s, and the concentrations of MDA8 O_3 in Beijing were relatively low on windy days. There was a high consistency between MDA8 O_3 in Beijing and the upwind region, suggesting that O_3 pollution may often be regional. It is noticeable that, especially under the southerly wind

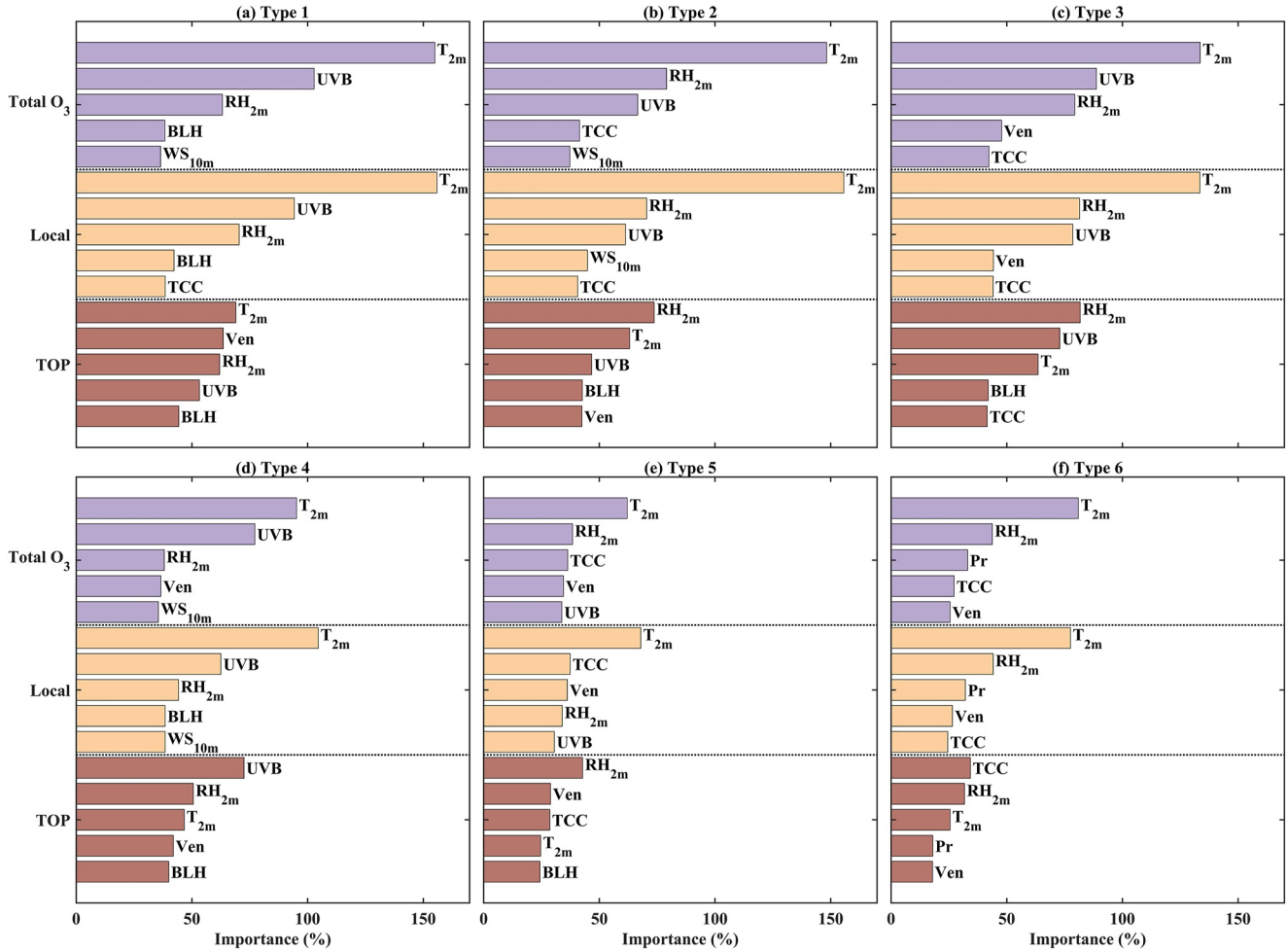

Figure 6. Top five most important variables affecting the O_3 concentration and local and TOP sources in Beijing under six patterns according to the RF model.

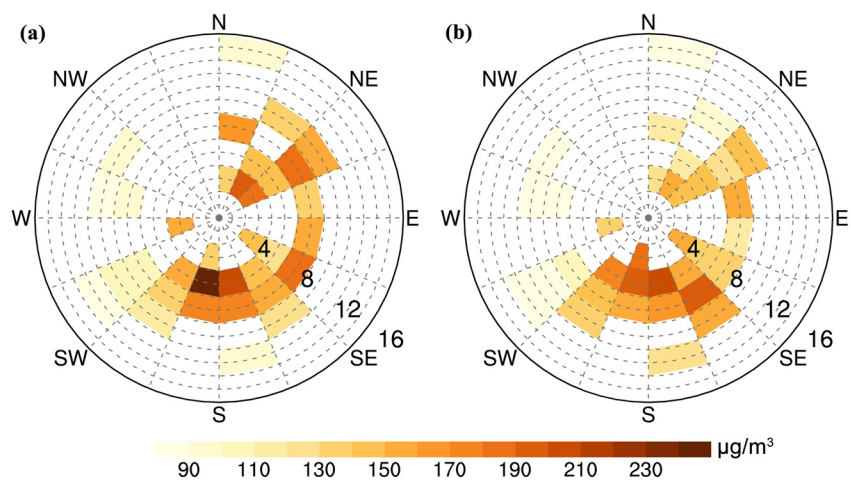

Figure 7. The MDA8 O_3 in Beijing (a) and the upwind region (b) under the dominant wind direction at 500 m from 2021-05-12 to 2021-07-12 (BJT).

scenario, with a higher O_3 concentration in Beijing, the O_3 concentration in the upwind region is also higher, where the more abundant O_3 in the upwind region will be transported to Beijing by the airflow, which confirms the transboundary transport contribution of southerly winds mentioned earlier. In the case of northeasterly winds, O_3 pollution in the upwind area was not as high as in Beijing, and coupled with the topographical obstruction, it was difficult for pollutants from the upwind area to be transported to Beijing. At this time, the local accumulation should be mainly responsible for the pollution in Beijing. During the observation period, two typical O_3 pollution events occurred in Beijing (Case 1: 2021-05-18–2021-05-22; Case 2: 2021-06-07–2021-06-08), including southerly winds and northeasterly winds, and we further explored the role played by local winds in these events.

3.2.1. Modulation of the Low-Level Jet

The low-level jet (LLJ) is a fast-moving stream that occurs in the lowest few kilometres of the atmosphere with maximum wind speed (Stensrud, 1996). Turbulent mixing resulting from wind shear below the jet plays an essential role in regulating the transport of heat, water vapor, and atmospheric pollutants (Darby et al., 2006; Miao et al., 2018; Patil et al., 2022; Yang et al., 2019, 2023). Generally, the LLJs over Beijing occur more frequently in spring and winter, which are usually induced by synoptic forcings, especially under synoptic patterns associated with strong southwest-to-northeast or southeast-to-northwest pressure gradient across Beijing (Miao et al., 2018). Indeed, the CDWL captured strong LLJs from 2021-5-18 21:20 BJT to 2021-5-20 00:00 BJT during Case 1 (Figures 8b and 8d), and the corresponding O_3 concentrations exceeded the pollution threshold. Before the formation of the LLJ (around 2021-5-18 14:00 BJT), the vertical mixing enhanced due to the gradual increase of low-level horizontal wind speed (Figures 8a and 8c), accompanied by a sudden decrease in O_3 concentration from 15:00 to 17:00 BJT. The strong southeast-to-northwest pressure gradient across Beijing was an important cause of the jet flow (Figure S10 in Supporting Information S1). In addition, the daytime LLJ for May 19th formed well before that morning, but LLJ were weakened around 2021-5-19 12:00 BJT until it redeveloped as the MLH dropped, indicating that the formation and disappearance of the LLJ are regulated by the diurnal evolution of the boundary layer (Blackadar, 1957). After sunset, photochemical reactions terminate and atmospheric NOx and CO titration reactions cause O_3 depletion, but O_3 concentrations suddenly increased at around 22:00, which we speculate was caused by the strengthened LLJ resulting in near-surface horizontal transport. As a consequence, we further discuss the variation in O_3 concentration at the closest environmental monitoring station (Yongledian; location: 116.30°N, 39.52°E) to Beijing Daxing International Airport, at an upwind station (3588A; location: 116.0901°N, 38.9816°E), and a downwind station (1003A; location: 116.339°N, 39.929°E) during the LLJ period.

The O_3 concentration at the upwind station was higher on May 18th, which supplied abundant sources for the horizontal transport of the LLJ. In particular, with the steady development of the nocturnal LLJ, the upwind station exhibited a faster decrease in O_3 concentration, and accordingly, the rates of decline in O_3 concentration at the local station (Yongledian) and downwind station slowed, and it was even the case that the O_3 concentration increased instead of decreased at around 22:00 (Figure 9a). Another explanation for the increase in nighttime O_3 is that a strong LLJ enhances vertical mixing and sinking air pulls the O_3 of the residual layer to the surface (X. M. Hu et al., 2013; Ma et al., 2013), but no obvious downdraft was captured before the O_3 increase in this process. After 2021-5-19 01:00 BJT, the O_3 concentration at the upwind station was already lower than at the local station and the downwind station. As a result of the development of the convective boundary layer, the height of the LLJ also rose continuously, sustaining at around 1–1.5 km above ground level in the afternoon (Figure 9b). The O_3 concentrations at the three stations showed relatively consistent variation before noon, with a small gradient between the stations, but gradually converted to a pattern of "upwind station < local station < downwind station" in the late afternoon. This is consistent with our previous comment that northern stations (i.e., the downwind station) may be more affected by the TOP from the south. Besides, it is worth mentioning that the peak O_3 concentration at the downwind station was also characterized by a lag of about 1 hr (Figure 9a). The photochemical reaction stopped after sunset, and the O_3 concentration gradient between the local station and the downwind station decreased. At 00:00 on May 20th, the LLJ weakened and atmospheric stability enhanced, and then the O_3 concentration difference between the local and downwind station was dominated by urban-rural differences in atmospheric components. The synoptic weather pattern of Case 1 was similar to that of Type 2 (Figure S10 in Supporting Information S1), and transboundary transport arising from the strong southerly LLJ within the boundary layer played a significant role in the O_3 pollution.

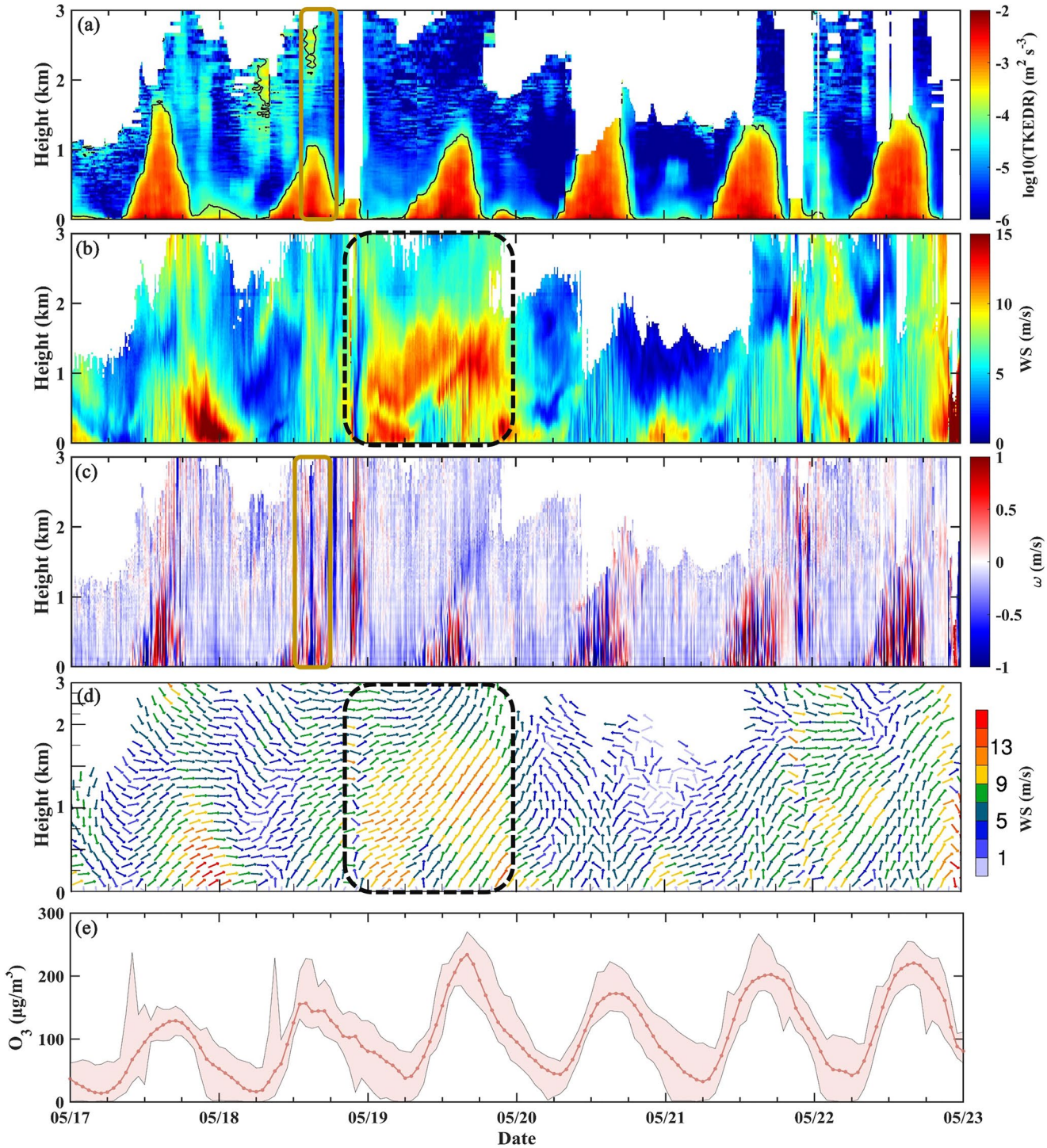

Figure 8. Boundary layer characteristics detected by CDWL from 17 to 23 May 2021 (Case 1): (a) $\log_{10}$(TKEDR), in which the black line indicates the TKEDR threshold of 10^{-4} m^2 s^{-3}; (b) horizontal wind speed; (c) vertical wind speed; (d) horizontal wind vectors. (e) Corresponding O_3 concentration variations, in which shading indicates the standard deviation. The solid brown box indicates the time from 2021-5-18 14:00 BJT to 2021-5-18 18:00 BJT, and the dashed black box indicates the time from 2021-5-18 21:20 BJT to 2021-5-20 00:00 BJT.

3.2.2. Impact of the Weak Wind Condition

On the afternoon of 8 June 2021, there was high-concentration O_3 pollution at ground level in Beijing, and the wind speeds within the boundary layer were relatively low. Weak southeasterly winds (<5 m/s) prevailed in the

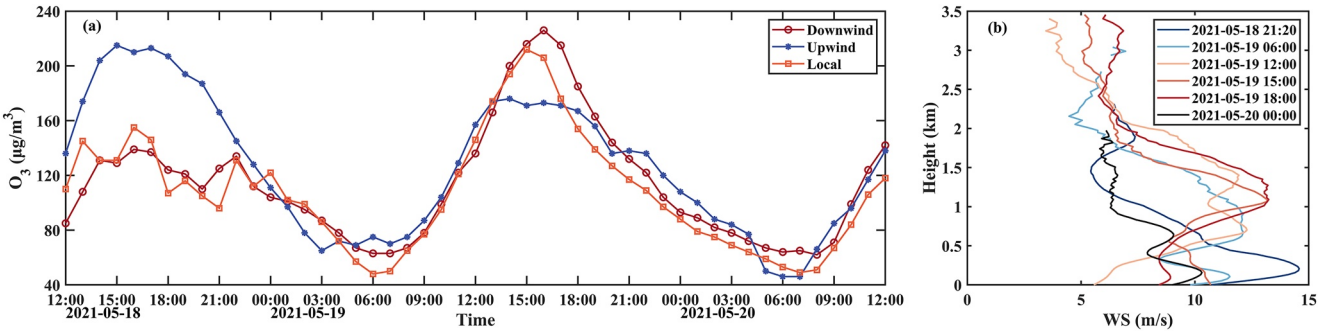

Figure 9. (a) The variation in O_3 concentration at the closest environmental monitoring station (Yongledian; location: 116.30°N, 39.52°E) to Beijing Daxing International Airport, an upwind station (3588A; location: 116.0901°N, 38.9816°E), and a downwind station (1003A; location: 116.339°N, 39.929°E) during the LLJ period. (b) Wind speed profile samples derived from CDWL.

near-surface layer below 1 km (Figure 10), so it can be presumed that TOP was not the main cause of this pollution. The distribution of surface O_3 concentrations on that day also showed a single island of pollution occurring in Beijing, with a particularly clean belt to the south of Beijing, which further confirms that this process was less influenced by transboundary transport (Figure S11 in Supporting Information S1). The 925-hPa atmospheric circulation of this process also provides further evidence that Beijing was within the uniform pressure field in front of the high pressure at 14:00 BJT on that day, and the weak wind zone within the boundary layer enveloped Beijing, which resembles Type 5 (Figure S12 in Supporting Information S1). The weak horizontal wind speed in the BTH region suppressed the horizontal transport of O_3 and its precursors to a large extent, and thus an isolated island pattern of O_3 pollution occurred in Beijing. Also, the TKEDR and vertical velocity on June 8th were stronger than those of the day before and after the O_3 pollution (Figures 10a and 10c), and nighttime O_3 in the residual layer may be carried to the ground by strong vertical mixing after sunrise to enhance pollution (J. Hu et al., 2018; Huang et al., 2021; Kaser et al., 2017). In short, a stable boundary layer and weak wind conditions provide favorable conditions for the accumulation of pollutants (Y. Liu & Wang, 2020; T. Wang et al., 2017; Xue et al., 2023), and once the abundant precursors have undergone photochemical reactions on sunny days, severe O_3 pollution occurs.

4. Discussion

As a secondary pollutant that is not emitted directly into the atmosphere, O_3 within the boundary layer has always been a complex and uncertain issue, and it is no exception when it comes to interpreting its transport mechanisms and understanding its sources. In this study, objective weather classification was applied to regional-scale boundary layer wind fields for all O_3 polluted days in Beijing during 2015–2021, and results showed that such classification based on the boundary layer wind field is capable of distinguishing the TOP characteristics well, including the transport source area, transport pathways, transport height, and how transport contributions vary with different circulation fields. Most previous studies have examined short-term pollution events or cases of pollution processes as examples (J. Hu et al., 2018; X. Wang et al., 2009; Zhang et al., 2022), and thus our understanding of TOP may be insufficient and biased. For instance, in the case of Beijing, there is a consensus that transboundary transport of O_3 is carried by prevailing southerly winds from places like Hebei, Henan, and Shandong Province (Ou et al., 2022; T. Wang et al., 2017). Our results show that, in addition to the transport caused by prevailing southerly winds, the eastward transport of O_3 and its precursors from Shanxi Province, attributable to westerly winds from the northwestern region, further enhances the O_3 level in Beijing. The other dual transport pathway is the combination of prevailing southeasterly and northeasterly winds that deliver abundant O_3 and precursors from upwind areas to Beijing (Figure 3, Figures S3 and S4 in Supporting Information S1). If the southwest airflow in the initial period transports O_3 pollution from the BTH region to the Bohai Sea as well as Liaoning Province, once the wind direction over the Bohai Sea turns to a prevailing easterly and northeasterly, winds will transport pollutants back to the BTH region (Zhang et al., 2022). Admittedly, our results also differentiate the circulation patterns for O_3 pollution events with weak transport, where unfavorable ventilation conditions in the BTH region lead to the accumulation of O_3 and precursors that increase O_3 concentrations (Y. Liu & Wang, 2020).

The backward trajectories simulated by the HYSPLIT model applying CWT analysis can successfully identify potential sources in spatial terms of TOP under different patterns well, which can further screen out the differences in transport source regions and distances under similar wind field patterns. For instance, for Type 1

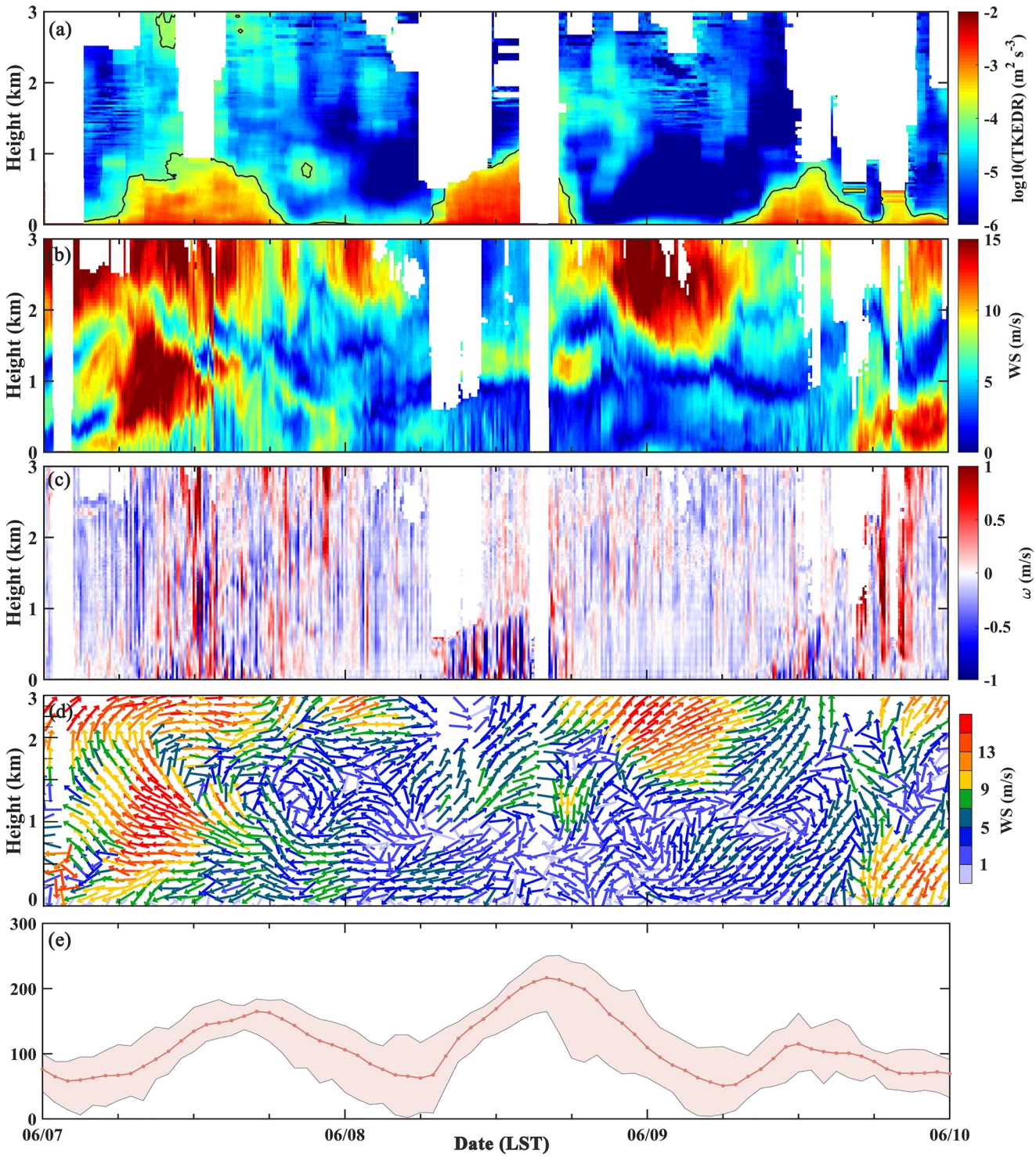

Figure 10. Same as Figure 8 but for Case 2 (from 7 to 9 June 2021).

and Type 2, although subjectively the regional-scale circulation patterns are quite similar (Figure S2 in Supporting Information S1), on the one hand, the location and strength of north-westerly and south-westerly wind shears to the west of Beijing affect the location of the pollutant transport source area, while on the other hand, the difference in wind speed magnitude to the south of Beijing is what regulates the distance of pollutant transport to the north (Figure 4). Apart from that, the transport heights of the north-westerly and westerly TOP are quite different

according to Figure S5 in Supporting Information S1, influenced by the topography and synoptic systems, and northwestern TOP (under Type 1) will occur at a higher altitude (approximately within 850–650 hPa) than the westerly TOP (under Type 2, below ~850 hPa). In brief, this scheme captures and distinguishes well the local and transboundary O_3 characteristics (including the transport source region, pathways, height, and distance) under various ventilation patterns. Again, this confirms the robustness and accuracy of objective weather classification in identifying the characteristics of the atmospheric circulation field.

This study utilized NMF based entirely on a mathematical (statistical) approach to extract the contributions of O_3 pollution sources in Beijing, without requiring large amounts of chemically speciated data. There is no doubt that NMF is a more effective and economical method for source decomposition in the face of long time-series historical observations of pollution data. According to a previous study based on chemical transport models, the monthly contributions of precursor emissions to O_3 in the receptor region proved that local sources constitute the major contributors to the BTH region (M. Y. Wang et al., 2019). The transport of pollutants from other regions accounted for 41.66% of the total O_3 on polluted days in Beijing (H. Liu et al., 2019); in particular, the contribution of TOP in Beijing urban areas can reach 70% of the regional O_3 and the rest of the precursor transport during an O_3 period (X. Wang et al., 2009). Our NMF results show that TOP was responsible for about 26.64% of total O_3 on average. Specifically, 27% of ventilation patterns had a TOP contribution of more than 40%, which is comparable to the above cases. Although NMF is a source decomposition method that relies completely on mathematical calculations, and compared to chemical transport models lacks consideration of source emissions and physicochemical processes, it is efficient and effective at assessing and providing great insight into the local accumulation and transportation of pollutants. Note that we preset the NMF factor to 2 due to the fact that the aim of this study was to shed light on the overall contribution of local sources and transport sources. If more detailed source decomposition needs to be considered, such as the contribution of precursor transport, the transport sources obtained from NMF can be subjected to NMF again. Indeed, Kim and Park (2007) proposed a procedure for calculating the dispersion coefficient to determine the number of NMF factors. We calculated the dispersion coefficients when the factor number was preset to 2 and other numbers, and the dispersion coefficient for 2 factors showed a higher value, which also strengthens the reasonableness and credibility. In addition, the NMF results also detected the effects on TOP of the location and subsurface properties of stations to some extent. The TOP contribution of the stations located in areas with high traffic volumes was lowest owing to more precursor emissions leading to dominant local sources, followed by urban stations. As Beijing is surrounded by mountains to the west, north and east, pollutants are prone to accumulate and it is hard for them to disperse to the downwind areas during prevailing southerly winds, especially for stations to the north.

To sum up, this study identified the sources of O_3 in Beijing from the perspective of transport and local accumulation. First, we are oriented by the weather circulation pattern associated with the variations in the boundary layer wind field, which distinguishes O_3 source induced by TOP and local accumulation in terms of weather mechanisms. In particular, the similar transport processes for O_3 and precursors can be categorized together based on T-PCA, but the detailed transport strengths and contributions need to be further determined. Then, the CWT analysis is applied to the classified backward trajectories, which contributed to the identification of potential source contributions of TOP in Beijing from upwind areas. By calculating the concentration weights of different trajectories, the pollution level of trajectories can be quantitatively obtained. In conjunction with the HYSPLIT model, the characteristics of the transport processes under different weather patterns have been well elucidated and summarized. It should also be noted that the limitation of this method is that it can only quantify the potential source contributions for different trajectories, but cannot determine the overall contribution of TOP to the pollution processes. However, the NMF we used answers exactly this question without requiring large amounts of chemically speciated data. On the other hand, NMF needs to be coupled with the subjective recognition of transported and local sources, whereas the previous results are well suited to inform the determination of the causes. With the interplay of the multiple methods, the results can scientifically and robustly shed light on the impacts of boundary layer ventilation on local and transboundary O_3 pollution patterns. In general, our study reveals the role of the boundary layer wind field in regulating O_3 pollution events and illustrates the horizontal transport characteristics under different synoptic patterns, providing a unique insight into the local accumulation and transport of air pollutants within the boundary layer. With the assistance of 3D wind field observations from CDWL, the important role of atmospheric ventilation in pollution events was further explored. Nevertheless, there are still flaws in the vertical dispersion of O_3 owing to a lack of vertical observations of O_3. Note that although the validation results of this study are slightly restricted to a single lidar observation, the majority of transboundary pollution in Beijing mainly is from southern cities, and the location of the CDWL is very prom-

ising for capturing the wind characteristics of the south-to-north transboundary pollution. For the processes dominated by TOP in other directions or local accumulation, it will be necessary to conduct lidar network observations of 3D wind fields in the different orientations of the city for mutual validation in the future. Since ventilation acts as a vital role in the transport of heat, air pollutants, moisture, and energy, the new integrated approaches and results could have important implications for pollution islands, urban heat islands in Beijing, or other megacities.

5. Conclusions

In this study, concerning O_3 pollution days in Beijing during 2015–2021, six types of ventilation conditions affecting O_3 pollution in Beijing were obtained by applying objective weather classification to their regional-scale boundary layer wind fields. The results indicated that horizontal wind field variations have significant modulating effects on local O_3 and TOP.

To sum up, local sources are the key contributors to O_3 pollution events in Beijing, accounting for about 73.36% of the O_3 concentration on average. Local meteorological conditions such as high temperatures, strong solar radiation, and fewer cloud cover are the major objective factors for the generation of O_3 pollution. Local transport is dominant when controlled by a uniform pressure field, and a stable boundary layer is conducive to enhanced accumulation of pollutants. By contrast, despite the smaller TOP contribution in the whole of Beijing, the TOP cannot be discounted owing to the more frequent occurrence of synoptic patterns associated with it. Regarding different wind patterns, the wind direction and wind speed of the horizontal wind field jointly drive the transport source region, pathways, height, and contributions for TOP. In addition to the southern TOP from Henan, Hebei, and Shandong Province, there are two other dual transport pathways in Beijing: (a) from Shanxi and Henan–Hebei brought by westerly and south-westerly wind shear; and (b) from Shandong–Hebei and southwestern Liaoning Province owing to the convergence of easterly and southeasterly currents caused by the western Pacific subtropical high and continental high. Generally, the transport height of northwestern TOP is lower than that of southern TOP. In detail, pollutants are predominantly transported to Beijing induced by prevailing southerly winds at a height equivalent to 850–1,000 hPa, while the maximum transport height of the northwestern TOP may extend from the surface to about 650 hPa. Additionally, the geographic location and urban surface characteristics play an essential role in the TOP differences among the 35 environmental monitoring stations in Beijing. Traffic stations correspond to more precursor emissions resulting in less impact of TOP; suburban and rural areas are more exposed to TOP impacts; and the influences of TOP gradually increase from south to north. For the stations to the north, the contribution of TOP may reach up to 56%.

Strong solar UV radiation and high temperatures are the key factors driving O_3 pollution events, followed by the BLH and wind speed affecting the horizontal transport of O_3 concentrations. Atmospheric ventilation and BLH are key drivers of TOP, while meteorological factors predominantly modulate local sources. Based on CDWL observations, we also found a transient increase in O_3 concentrations as a result of the nighttime LLJ (with maximum wind speed >10 m/s) leading to the transport of pollutants to Beijing; however, the daytime LLJ contributes to a lag of about 1 hr in the peak O_3 concentration in the downwind region. Besides, Beijing may be enveloped by a large area of weak winds (~3 m/s) under the control of a uniform pressure field; the weak horizontal wind speed in the BTH region suppresses the horizontal transport of O_3 and its precursors to a large extent, in which case Beijing may become a separate pollution island.

Overall, our findings are not only meaningful for the prediction and assessment of O_3 pollution formation but also in providing a new perspective and idea regarding the dispersion and transport of other atmospheric pollutants, as well as revealing the non-negligible role of boundary layer atmospheric ventilation in the formation of atmospheric pollution in a more holistic and detailed way. Future research should be conducted when more refined 3D air quality data become available (C. Liu et al., 2021), thus providing a more comprehensive understanding of the effects of boundary layer atmospheric ventilation on air quality.

Conflict of Interest

The authors declare no conflicts of interest relevant to this study.

Data Availability Statement

The data sets that are analyzed and used to support the findings of this study are available in the public domains: The ground-level O_3, NO_2, and CO observation data and the hourly meteorological data are deposited at linkage: https://doi.org/10.5281/zenodo.8271546 (Zong, 2023). The ERA5 reanalysis data set is available at the European Centre for Medium-Range Weather Forecasts (https://doi.org/10.24381/cds.bd0915c6; Hersbach et al., 2023).

Acknowledgments
This research was supported by the National Natural Science Foundation of China (42222503 and 42175098).

References

Atkinson, R. W., Yu, D., Armstrong, B. G., Pattenden, S., Wilkinson, P., Doherty, R. M., et al. (2012). Results from five urban and five rural U. K. populations. *Environmental Health Perspectives*, *120*(10), 1411–1417. https://doi.org/10.1289/ehp.1104108

Banakh, V. A., & Smalikho, I. N. (2018). Lidar studies of wind turbulence in the stable atmospheric boundary layer. *Remote Sensing*, *10*(8), 1219. https://doi.org/10.3390/rs10081219

Banakh, V. A., Smalikho, I. N., & Falits, A. V. (2020). Estimation of the height of the turbulent mixing layer from data of Doppler lidar measurements using conical scanning by a probe beam. *Atmospheric Measurement Techniques*, *14*(2), 1511–1524. https://doi.org/10.5194/amt-14-1511-2021

Blackadar, A. K. (1957). Boundary layer wind maxima and their significance for the growth of nocturnal inversions. *Bulletin of the American Meteorological Society*, *38*(5), 283–290. https://doi.org/10.1175/1520-0477-38.5.283

Brunet, J. P., Tamayo, P., Golub, T. R., & Mesirov, J. P. (2004). Metagenes and molecular pattern discovery using matrix factorization. *Proceedings of the National Academy of Sciences of the United States of America*, *101*(12), 4164–4169. https://doi.org/10.1073/pnas.0308531101

Chen, W., Wang, W., Jia, S., Mao, J., Yan, F., Zheng, L., et al. (2022). A new index developed for fast diagnosis of meteorological roles in ground-level ozone variations. *Advances in Atmospheric Sciences*, *39*(3), 403–414. https://doi.org/10.1007/s00376-021-1257-x

Chen, S., Yang, Y., Deng, F., Zhang, Y., Liu, D., Liu, C., & Gao, Z. (2022). A high-resolution monitoring approach of canopy urban heat island using a random forest model and multi-platform observations. *Atmospheric Measurement Techniques*, *15*(3), 735–756. https://doi.org/10.5194/amt-15-735-2022

Darby, L. S., Allwine, K. J., & Banta, R. M. (2006). Nocturnal low-level jet in a mountain basin complex. Part II: Transport and diffusion of tracer under stable conditions. *Journal of Applied Meteorology and Climatology*, *45*(5), 740–753. https://doi.org/10.1175/JAM2367.1

Deng, T., Wang, T., Wang, S., Zou, Y., Yin, C., Li, F., et al. (2019). Impact of typhoon periphery on high ozone and high aerosol pollution in the Pearl River Delta region. *Science of the Total Environment*, *668*, 617–630. https://doi.org/10.1016/j.scitotenv.2019.02.450

Dong, Y., Li, J., Guo, J., Jiang, Z., Chu, Y., Chang, L., et al. (2020). *The impact of synoptic patterns on summertime ozone pollution in the North China Plain*. Science of the Total Environment. https://doi.org/10.1016/j.scitotenv.2020.139559.139559

Foley, K. M., Hogrefe, C., Pouliot, G., Possiel, N., Roselle, S. J., Simon, H., & Timin, B. (2015). Dynamic evaluation of CMAQ Part I: Separating the effects of changing emissions and changing meteorology on ozone levels between 2002 and 2005 in the eastern US. *Atmospheric Environment*, *103*(x), 247–255. https://doi.org/10.1016/j.atmosenv.2014.12.038

Fu, Y., Liao, H., & Yang, Y. (2019). Interannual and decadal changes in tropospheric ozone in China and the associated chemistry-climate interactions: A review. *Advances in Atmospheric Sciences*, *36*(9), 975–993. https://doi.org/10.1007/s00376-019-8216-9

Gvozdić, V., Kovač-Andrić, E., & Brana, J. (2011). Influence of meteorological Factors NO_2, SO_2, CO and PM10 on the concentration of O_3 in the urban atmosphere of Eastern Croatia. *Environmental Modeling & Assessment*, *16*(5), 491–501. https://doi.org/10.1007/s10666-011-9256-4

Han, H., Liu, J., Shu, L., Wang, T., & Yuan, H. (2020). Local and synoptic meteorological influences on daily variability in summertime surface ozone in eastern China. *Atmospheric Chemistry and Physics*, *20*(1), 203–222. https://doi.org/10.5194/acp-20-203-2020

Heal, M. R., Heaviside, C., Doherty, R. M., Vieno, M., Stevenson, D. S., & Vardoulakis, S. (2013). Health burdens of surface ozone in the UK for a range of future scenarios. *Environment International*, *61*, 36–44. https://doi.org/10.1016/j.envint.2013.09.010

Hersbach, H., Bell, B., Berrisford, P., Biavati, G., Horányi, A., Muñoz Sabater, J., et al. (2023). ERA5 hourly data on pressure levels from 1940 to present [Dataset]. Copernicus Climate Change Service (C3S) Climate Data Store (CDS). https://doi.org/10.24381/cds.bd0915c6

Hu, J., Li, Y., Zhao, T., Liu, J., Hu, X. M., Liu, D., et al. (2018). An important mechanism of regional O_3 transport for summer smog over the Yangtze River Delta in eastern China. *Atmospheric Chemistry and Physics*, *18*(22), 16239–16251. https://doi.org/10.5194/acp-18-16239-2018

Hu, X. M., Klein, P. M., Xue, M., Zhang, F., Doughty, D. C., Forkel, R., et al. (2013). Impact of the vertical mixing induced by low-level jets on boundary layer ozone concentration. *Atmospheric Environment*, *70*, 123–130. https://doi.org/10.1016/j.atmosenv.2012.12.046

Huang, T., Yang, Y., O'Connor, E. J., Lolli, S., Haywood, J., Osborne, M., et al. (2021). Influence of a weak typhoon on the vertical distribution of air pollution in Hong Kong: A perspective from a Doppler LiDAR network. *Environmental Pollution*, *276*, 116534. https://doi.org/10.1016/j.envpol.2021.116534

Huth, R. (2000). A circulation classification scheme applicable in GCM studies. *Theoretical and Applied Climatology*, *67*(1–2), 1–18. https://doi.org/10.1007/s007040070012

Huth, R., Beck, C., Philipp, A., Demuzere, M., Ustrnul, Z., Cahynová, M., et al. (2008). Classifications of atmospheric circulation patterns: Recent advances and applications. *Annals of the New York Academy of Sciences*, *1146*(1), 105–152. https://doi.org/10.1196/annals.1446.019

Kaser, L., Patton, E. G., Pfister, G. G., Weinheimer, A. J., Montzka, D. D., Flocke, F., et al. (2017). The effect of entrainment through atmospheric boundary layer growth on observed and modeled surface ozone in the Colorado Front Range. *Journal of Geophysical Research*, *122*(11), 6075–6093. https://doi.org/10.1002/2016JD026245

Kim, H., & Park, H. (2007). Sparse non-negative matrix factorizations via alternating non-negativity-constrained least squares for microarray data analysis. *Bioinformatics*, *23*(12), 1495–1502. https://doi.org/10.1093/bioinformatics/btm134

Kley, D., Geiss, H., & Mohnen, V. A. (1994). Tropospheric ozone at elevated sites and precursor emissions in the United States and Europe. *Atmospheric Environment*, *28*(1), 149–158. https://doi.org/10.1016/1352-2310(94)90030-2

Kolmogorov, A. N. (1991). The local structure of turbulence in incompressible viscous fluid for very large Reynolds numbers. *Proceedings of the Royal Society of London. Series A: Mathematical and Physical Sciences*, *434*, 9–13. https://doi.org/10.1098/rspa.1991.0075

Lam, K. S., Wang, T. J., Wu, C. L., & Li, Y. S. (2005). Study on an ozone episode in hot season in Hong Kong and transboundary air pollution over Pearl River Delta region of China. *Atmospheric Environment*, *39*(11), 1967–1977. https://doi.org/10.1016/j.atmosenv.2004.11.023

Lee, D. D., & Seung, H. S. (1999). Learning the parts of objects by non-negative matrix factorization. *Nature*, *401*(6755), 788–791. https://doi.org/10.1038/44565

Liu, C., Gao, M., Hu, Q., Brasseur, G. P., & Carmichael, G. R. (2021). Stereoscopic monitoring: A promising strategy to advance diagnostic and prediction of air pollution. *Bulletin of the American Meteorological Society*, *102*(4), E730–E737. https://doi.org/10.1175/BAMS-D-20-0217.1

Liu, C., Xing, C., Hu, Q., Li, Q., Liu, H., Hong, Q., et al. (2022). Ground-based hyperspectral stereoscopic remote sensing network: A promising strategy to learn coordinated control of O_3 and $PM_{2.5}$ over China. *Engineering*, *19*, 71–83. https://doi.org/10.1016/j.eng.2021.02.019

Liu, H., Zhang, M., Han, X., Li, J., & Chen, L. (2019). Episode analysis of regional contributions to tropospheric ozone in Beijing using a regional air quality model. *Atmospheric Environment*, *199*, 299–312. https://doi.org/10.1016/j.atmosenv.2018.11.044

Liu, Y., & Wang, T. (2020). Worsening urban ozone pollution in China from 2013 to 2017 - Part 2: The effects of emission changes and implications for multi-pollutant control. *Atmospheric Chemistry and Physics*, *20*(11), 6323–6337. https://doi.org/10.5194/acp-20-6323-2020

Lu, X., Hong, J., Zhang, L., Cooper, O. R., Schultz, M. G., Xu, X., et al. (2018). Severe surface ozone pollution in China: A global perspective. *Environmental Science and Technology Letters*, *5*(8), 487–494. https://doi.org/10.1021/acs.estlett.8b00366

Lu, X., Zhang, L., Chen, Y., Zhou, M., Zheng, B., Li, K., et al. (2019). Exploring 2016-2017 surface ozone pollution over China: Source contributions and meteorological influences. *Atmospheric Chemistry and Physics*, *19*(12), 8339–8361. https://doi.org/10.5194/acp-19-8339-2019

Luo, M., Hou, X., Gu, Y., Lau, N. C., & Yim, S. H. L. (2018). Trans-boundary air pollution in a city under various atmospheric conditions. *Science of the Total Environment*, *618*, 132–141. https://doi.org/10.1016/j.scitotenv.2017.11.001

Luo, Y., Zhao, T., Yang, Y., Zong, L., Kumar, K. R., Wang, H., et al. (2022). Seasonal changes in the recent decline of combined high $PM_{2.5}$ and O_3 pollution and associated chemical and meteorological drivers in the Beijing–Tianjin–Hebei region, China. *Science of the Total Environment*, *838*, 156312. https://doi.org/10.1016/j.scitotenv.2022.156312

Ma, Z., Xu, H., Meng, W., Zhang, X., Xu, J., Liu, Q., & Wang, Y. (2013). Vertical ozone characteristics in urban boundary layer in Beijing. *Environmental Monitoring and Assessment*, *185*(7), 5449–5460. https://doi.org/10.1007/s10661-012-2958-5

Malley, C. S., Braban, C. F., & Heal, M. R. (2014). The application of hierarchical cluster analysis and non-negative matrix factorization to European atmospheric monitoring site classification. *Atmospheric Research*, *138*, 30–40. https://doi.org/10.1016/j.atmosres.2013.10.019

Miao, Y., Guo, J., Liu, S., Liu, H., Li, Z., Zhang, W., & Zhai, P. (2017). Classification of summertime synoptic patterns in Beijing and their associations with boundary layer structure affecting aerosol pollution. *Atmospheric Chemistry and Physics*, *17*(4), 3097–3110. https://doi.org/10.5194/acp-17-3097-2017

Miao, Y., Guo, J., Liu, S., Wei, W., Zhang, G., Lin, Y., & Zhai, P. (2018). The climatology of low-level jet in Beijing and Guangzhou, China. *Journal of Geophysical Research: Atmospheres*, *123*(5), 2816–2830. https://doi.org/10.1002/2017JD027321

Ning, G., Yim, S. H. L., Wang, S., Duan, B., Nie, C., Yang, X., et al. (2019). Synergistic effects of synoptic weather patterns and topography on air quality: A case of the Sichuan Basin of China. *Climate Dynamics*, *53*(11), 6729–6744. https://doi.org/10.1007/s00382-019-04954-3

Ou, S., Wei, W., Cheng, S., & Cai, B. (2022). Exploring drivers of the aggravated surface O_3 over North China Plain in summer of 2015 – 2019: Aerosols, precursors, and meteorology. *Journal of Environmental Sciences*, *127*, 453–464. https://doi.org/10.1016/j.jes.2022.06.023

Pancholi, P., Kumar, A., Bikundia, D. S., & Chourasiya, S. (2018). An observation of seasonal and diurnal behavior of O_3–NOx relationships and local/regional oxidant ($O_X = O_3 + NO_2$) levels at a semi-arid urban site of western India. *Sustainable Environment Research*, *28*(2), 79–89. https://doi.org/10.1016/j.serj.2017.11.001

Patil, C., Malap, N., Sathyanadh, A., Balaji, B., Prabhakaran, T., & Karipot, A. (2022). Moisture transport enhanced by the nocturnal low-level jet in association with the passage of a monsoon depression over the Indian subcontinent. *Atmospheric Research*, *272*, 106123. https://doi.org/10.1016/j.atmosres.2022.106123

Qi, M., Zhu, B., Pan, C., & Su, J.-F. (2015). Regional differences and meteorological conditions of a low visibility procedure over the Yangtze River Delta Region in winter. *China Environmental Ence*, *35*(10), 2899–2907. https://doi.org/10.3969/j.issn.1000-6923.2015.10.003

Shao, M., Yang, J., Wang, J., Chen, P., Liu, B., & Dai, Q. (2022). Co-occurrence of surface O_3, $PM_{2.5}$ pollution, and tropical cyclones in China. *Journal of Geophysical Research: Atmospheres*, *127*(14). https://doi.org/10.1029/2021JD036310

Shu, L., Wang, T., Xie, M., Li, M., Zhao, M., Zhang, M., & Zhao, X. (2019). Episode study of fine particle and ozone during the CAPUM-YRD over Yangtze River Delta of China: Characteristics and source attribution. *Atmospheric Environment*, *203*, 87–101. https://doi.org/10.1016/j.atmosenv.2019.01.044

Sillman, S. (1999). The relation between ozone, NOx and hydrocarbons in urban and polluted rural environments. *Developments in Environmental Science*, *33*(12), 1821–1845. https://doi.org/10.1016/S1474-8177(02)80015-8

Smalikho, I. N., & Banakh, V. A. (2017). Measurements of wind turbulence parameters by a conically scanning coherent Doppler lidar in the atmospheric boundary layer. *Atmospheric Measurement Techniques*, *10*(11), 4191–4208. https://doi.org/10.5194/amt-10-4191-2017

Song, C., Wu, L., Xie, Y., He, J., Chen, X., Wang, T., et al. (2017). Air pollution in China: Status and spatiotemporal variations. *Environmental Pollution*, *227*, 334–347. https://doi.org/10.1016/j.envpol.2017.04.075

Stensrud, D. J. (1996). Importance of low-level jets to climate: A review. *Journal of Climate*, *9*(8), 1698–1711. https://doi.org/10.1175/1520-0442(1996)009<1698:IOLLJT>2.0.CO;2

Wang, F., Chen, D. S., Cheng, S. Y., Li, J. B., Li, M. J., & Ren, Z. H. (2010). Identification of regional atmospheric PM10 transport pathways using HYSPLIT, MM5-CMAQ and synoptic pressure pattern analysis. *Environmental Modelling & Software*, *25*(8), 927–934. https://doi.org/10.1016/j.envsoft.2010.02.004

Wang, H., Li, J., Gao, Z., Yim, S. H. L., Shen, H., Ho, H. C., et al. (2019). High-spatial-resolution population exposure to PM2.5 pollution based on multi-satellite retrievals: A case study of seasonal variation in the Yangtze River Delta, China in 2013. *Remote Sensing*, *11*(23), 2724. https://doi.org/10.3390/rs11232724

Wang, L., Qiang, W., Xia, H., Wei, T., Yuan, J., & Jiang, P. (2021). Robust solution for boundary layer height detections with coherent Doppler wind Lidar. *Advances in Atmospheric Sciences*, *38*(11), 1920–1928. https://doi.org/10.1007/s00376-021-1068-0

Wang, M. Y., Yim, S. H. L., Dong, G. H., Ho, K. F., & Wong, D. C. (2020). *Mapping ozone source-receptor relationship and apportioning the health impact in the Pearl River Delta region using adjoint sensitivity analysis* (Vol. 222). Atmospheric Environment. https://doi.org/10.1016/j.atmosenv.2019.117026

Wang, M. Y., Yim, S. H. L., Wong, D. C., & Ho, K. F. (2019). Source contributions of surface ozone in China using an adjoint sensitivity analysis. *Science of the Total Environment*, *662*, 385–392. https://doi.org/10.1016/j.scitotenv.2019.01.116

Wang, N., Huang, X., Xu, J., Wang, T., Tan, Z. M., & Ding, A. (2022). Typhoon-boosted biogenic emission aggravates cross-regional ozone pollution in China. *Science Advances*, *8*(2). https://doi.org/10.1126/sciadv.abl6166

Wang, T., Xue, L., Brimblecombe, P., Lam, Y. F., Li, L., & Zhang, L. (2017). Ozone pollution in China: A review of concentrations, meteorological influences, chemical precursors, and effects. *Science of the Total Environment*, *575*, 1582–1596. https://doi.org/10.1016/j.scitotenv.2016.10.081

Wang, X., Li, J., Zhang, Y., Xie, S., & Tang, X. (2009). Ozone source attribution during a severe photochemical smog episode in Beijing, China. *Science in China, Series B: Chemistry*, *52*(8), 1270–1280. https://doi.org/10.1007/s11426-009-0137-5

Wang, Y. Q., Zhang, X. Y., & Draxler, R. R. (2009). TrajStat: GIS-based software that uses various trajectory statistical analysis methods to identify potential sources from long-term air pollution measurement data. *Environmental Modelling & Software*, *24*(8), 938–939. https://doi.org/10.1016/j.envsoft.2009.01.004

WHO (2021). WHO global air quality guidelines. Particulate matter (PM2.5 and PM10), ozone, nitrogen dioxide, sulfur dioxide and carbon monoxide.

Xiao, Q., Chang, H. H., Geng, G., & Liu, Y. (2018). An ensemble machine-learning model to predict historical PM2.5 concentrations in China from satellite data. *Environmental Science and Technology*, *52*(22), 13260–13269. https://doi.org/10.1021/acs.est.8b02917

Xue, J., Zong, L., Yang, Y., Bi, X., Zhang, Y., & Zhao, M. (2023). Diurnal and interannual variations of canopy urban heat island (CUHI) effects over a mountain–valley city with a semi-arid climate. *Urban Climate*, *48*, 101425. https://doi.org/10.1016/j.uclim.2023.101425

Yang, Y., Guo, M., Ren, G., Liu, S., Zong, L., Zhang, Y., et al. (2022). Modulation of wintertime canopy urban heat island (CUHI) intensity in Beijing by synoptic weather pattern in planetary boundary layer. *Journal of Geophysical Research: Atmospheres*, *127*(8), e2021JD035988. https://doi.org/10.1029/2021jd035988

Yang, Y., Guo, M., Wang, L., Zong, L., Liu, D., Zhang, W., et al. (2023). Unevenly spatiotemporal distribution of urban excess warming in coastal Shanghai megacity, China: Roles of geophysical environment, ventilation and sea breezes. *Building and Environment*, *235*, 110180. https://doi.org/10.1016/j.buildenv.2023.110180

Yang, Y., Wang, R., Chen, F., Liu, C., Bi, X., & Huang, M. (2021). Synoptic weather patterns modulate the frequency, type and vertical structure of summer precipitation over Eastern China: A perspective from GPM observations. *Atmospheric Research*, *249*, 105342. https://doi.org/10.1016/j.atmosres.2020.105342

Yang, Y., Yim, S. H. L., Haywood, J., Osborne, M., Chan, J. C. S., Zeng, Z., & Cheng, J. C. H. (2019). Characteristics of heavy particulate matter pollution events over Hong Kong and their relationships with vertical wind profiles using high-time-resolution Doppler lidar measurements. *Journal of Geophysical Research: Atmospheres*, *124*(16), 9609–9623. https://doi.org/10.1029/2019jd031140

Yang, Y., Zheng, X., Gao, Z., Wang, H., Wang, T., Li, Y., et al. (2018). Long-term trends of persistent synoptic circulation events in planetary boundary layer and their relationships with haze pollution in winter half year over eastern China. *Journal of Geophysical Research: Atmospheres*, *123*(19), 10991–11007. https://doi.org/10.1029/2018jd028982

Yin, Z., Cao, B., & Wang, H. (2019). Dominant patterns of summer ozone pollution in eastern China and associated atmospheric circulations. *Atmospheric Chemistry and Physics*, *19*(22), 13933–13943. https://doi.org/10.5194/acp-19-13933-2019

Yuan, J., Su, L., Xia, H., Li, Y., Zhang, M., Zhen, G., & Li, J. (2022). Microburst, windshear, gust front, and vortex detection in mega airport using a single coherent Doppler wind Lidar. *Remote Sensing*, *14*(7), 1–14. https://doi.org/10.3390/rs14071626

Yue, X., Unger, N., Harper, K., Xia, X., Liao, H., Zhu, T., et al. (2017). Ozone and haze pollution weakens net primary productivity in China. *Atmospheric Chemistry and Physics*, *17*(9), 6073–6089. https://doi.org/10.5194/acp-17-6073-2017

Zeng, Z., Wang, Z., Gui, K., Yan, X., Gao, M., Luo, M., et al. (2020). Daily global solar radiation in China estimated from high-density meteorological observations: A random forest model framework. *Earth and Space Science*, *7*(2). https://doi.org/10.1029/2019EA001058

Zhang, Y., Yu, S., Chen, X., Li, Z., Li, M., Song, Z., et al. (2022). Local production, downward and regional transport aggravated surface ozone pollution during the historical orange-alert large-scale ozone episode in eastern China. *Environmental Chemistry Letters*, *20*(3), 1577–1588. https://doi.org/10.1007/s10311-022-01421-0

Zhao, C., Wang, Y., Yang, Q., Fu, R., Cunnold, D., & Choi, Y. (2010). Impact of East Asian summer monsoon on the air quality over China: View from space. *Journal of Geophysical Research*, *115*(9), 1–12. https://doi.org/10.1029/2009JD012745

Zhao, Z., & Wang, Y. (2017). Influence of the West Pacific subtropical high on surface ozone daily variability in summertime over eastern China. *Atmospheric Environment*, *170*, 197–204. https://doi.org/10.1016/j.atmosenv.2017.09.024

Zong, L. (2023). Ground-based observation data from the article " elucidating the impacts of various atmospheric ventilation conditions on local and transboundary ozone pollution patterns: A case study of Beijing, China" [Dataset]. Zenodo. https://doi.org/10.5281/zenodo.8271546

Zong, L., Yang, Y., Gao, M., Wang, H., Wang, P., Zhang, H., et al. (2021). Large-scale synoptic drivers of co-occurring summertime ozone and $PM_{2.5}$ pollution in eastern China. *Atmospheric Chemistry and Physics*, *21*(11), 9105–9124. https://doi.org/10.5194/acp-21-9105-2021

Zong, L., Yang, Y., Xia, H., Gao, M., Sun, Z., Zheng, Z., et al. (2022). Joint occurrence of heatwaves and ozone pollution and increased health risks in Beijing, China: Role of synoptic weather pattern and urbanization. *Atmospheric Chemistry and Physics*, *22*(10), 6523–6538. https://doi.org/10.5194/acp-22-6523-2022